

# Updates on SM predictions of $|V_{cb}|$ and $R(D^*)$ in $B \rightarrow D^* \ell \nu_\ell$ decays

Sneha Jaiswal\* and Soumitra Nandi†

*Indian Institute of Technology, North Guwahati, Guwahati 781039, Assam, India*

Sunando Kumar Patra‡

*Indian Institute of Technology, North Guwahati, Guwahati 781039, Assam, India and  
Department of Physics, Bangabasi Evening College,  
19 Rajkumar Chakraborty Sarani, Kolkata 700009, West Bengal, India*

We update the standard model (SM) predictions of  $R(D^*)$  using the latest results on the decay distributions in  $B \rightarrow D^* \ell \nu_\ell$  ( $\ell = \mu, e$ ) by Belle collaboration, while extracting  $|V_{cb}|$  at the same time. Depending on the inputs used in the analysis, we define various fit scenarios. Although the central values of the predicted  $R(D^*)$  in all the scenarios have reduced from its earlier predictions in 2017, the results are consistent with each other within the uncertainties. In this analysis, our prediction of  $R(D^*)$  is consistent with the respective world average at  $\sim 3\sigma$ . We have also predicted several angular observables associated with  $B \rightarrow D^* \tau \nu_\tau$  decays. We note that the predicted  $F_L(D^*)$  is consistent with the corresponding measurement at  $2\sigma$ . Utilizing these new results, we fit the Wilson coefficients appearing beyond the standard model of particle physics (BSM). To see the trend of SM predictions, we have utilized the recently published preliminary results on the form-factors at non-zero recoil by the lattice groups like Fermilab-MILC and JLQCD and predicted the observables in  $B \rightarrow D^* \ell \nu_\ell$ , and  $B \rightarrow D^* \tau \nu_\tau$  decays.

## I. INTRODUCTION

Precise extraction of the CKM element  $|V_{cb}|$  is an important goal of the  $B$ -physics phenomenology. Inclusive and exclusive tree level semileptonic decays  $b \rightarrow c \ell \nu_\ell$  ( $\ell = e, \mu$ ) are crucial in this regard. Note that the inclusive and exclusive determinations of  $|V_{cb}|$  differ by  $\sim 3\sigma$  [1–3]. We will focus on the exclusive determination of  $V_{cb}$  from  $B \rightarrow D^{(*)} \ell \nu$  decays in this work. Other related observables like  $R(D^{(*)}) = \frac{Br(B \rightarrow D^{(*)} \tau \nu_\tau)}{Br(B \rightarrow D^{(*)} \ell \nu)}$  are useful for the test of lepton universality. Significant deviations from their respective SM predictions will be a clear signal for the lepton universality violating (LUV) new physics (NP). Precise prediction of these observables, thus, is of utmost importance.

In addition to the considerable improvements in the lattice determination of the form factors in the last decade [4–6], updated results on the branching fractions  $Br(B \rightarrow D^{(*)} \ell \nu)$  in different  $q^2$ -bins are now available [7]. With these new inputs, several groups had reanalyzed these decay modes using the Boyd-Grinstein-Lebed (BGL) [8] and Caprini-Lellouch-Neubert (CLN) [9] parametrizations for the form-factors. The latter uses heavy quark effective theory (HQET) relations between the form-factors in which relevant higher-order corrections are missing. The extracted values of  $|V_{cb}|$  and  $R(D^{(*)})$  have improved over their earlier estimates. For details, see [10–15] and the references therein. The world averages based on these analysis can be seen from ref. [16]:

$$R(D) = 0.299 \pm 0.003, \quad R(D^*) = 0.258 \pm 0.005, \quad |V_{cb}|^{exl} = (41.9 \pm 2.0) \times 10^{-3}. \quad (1)$$

Uncertainties in  $R(D^*)$  are estimated by parametrizing the missing higher-order pieces in the relations between the HQET form-factors [14, 15]. In all of those analyses, the ratios of the HQET form-factors are considered at order  $\mathcal{O}(\alpha_s, \frac{1}{m_b}, \frac{1}{m_c})$ . In the ref. [15], an additional correction of  $\approx 20\%$  between the ratios of the HQET form-factors is considered. Also, several different normalizations for the ratios of the form-factors  $F_2(w)/F_i(w)$  were used to predict  $R(D^*)$  and the variations in  $R(D^*)$  due to those were noted. Finding a method of predicting  $R(D^*)$  independent of the inputs from HQET is important and lattice inputs on the form-factors at non-zero recoil are required for that.

Very recently, Belle has updated their measurement on the decay distributions in  $B \rightarrow D^* \ell \nu_\ell$  [17]. They have also extracted the values of  $|V_{cb}|$  using the CLN and BGL parametrizations of the form-factors and the results are consistent with each other within the error-bars. The extracted value is lower than what was observed with their 2017 data (eq. 1). These new results from Belle are incorporated in a couple of other analyses [18, 19] where the

---

\*Electronic address: sneha.jaiswal@iitg.ac.in

†Electronic address: soumitra.nandi@iitg.ac.in

‡Electronic address: sunando.patra@gmail.com

authors have updated the prediction of  $R(D^*)$  in the SM. In both of these analyses, the predicted values of  $R(D^*)$  are consistent with the one given in eq. 1, but the central values are lowered by  $\approx 2\%$ . In ref. [19], the available results on  $B \rightarrow D^*$  form-factors from light-cone sum rule (LCSR) [20] at  $q^2 \neq 0$  are used.

In the present article, we have updated our earlier analysis [15] with the new inputs and have modified the method of our data-analysis. We know that the statistical analyses play an important role in addressing research questions. The two prevalent philosophies in inferential statistics are frequentist and Bayesian. The differences between these two frameworks originate from the way the concept of probability itself is interpreted. In our earlier publication, we had used frequentist framework in analyzing the data, where a parameter of interest is assumed to be unknown, but fixed (has a true value). In general, it is assumed that there is only one true regression coefficient in the population. Here, we have updated our method to the Bayesian view of subjective probability, where all unknown parameters are treated as uncertain and thus should be described in terms of their underlying probability distribution.

We would like to point out that in our earlier analysis we truncated the BGL series of all the relevant form-factors at  $N = 2$  which gave us stable results on the extracted  $V_{cb}$ . In such cases, the number of BGL parameters, associated with the three form-factors in  $B \rightarrow D^*$  decays, will be 9. In a recent work [21], it is shown that at the present level of precision the optimal number of BGL parameters required to fit the current data is less than 9. However, in such scenarios, the extracted values of  $V_{cb}$  will not be stable anymore. Although this is not our main focus, here we have pointed out the use of Akaike Information Theoretic approach (AIC) to find out optimal number of BGL coefficients which can best explain the data. The uses of AIC in the context of NP model selection can be seen from [22–24] and the references therein.

Along with the extraction of  $|V_{cb}|$  and the prediction of  $R(D^*)$ , we have extracted a few angular observables related to  $B \rightarrow D^* \tau \nu_\tau$  decays. Also, the variation of the form-factors, and the decay rate distributions with the recoil angle  $w$  are shown. The results are compared with those obtained from the old Belle data [7] and we have noted a shift in the distributions. As before, the updated SM prediction for  $R(D^*)$  show deviations from its measured value [16]. The presence of new interactions beyond the SM can explain this deviation. Regarding this, there are plenty of analyses available in the literature. Here, we would like to point out a few references where bounds on model-independent new WCs are obtained using the updated results in 2017 [24–30]. In this article, we extract the model-independent new physics Wilson coefficients (WC) using these newly available inputs.

Recently, a set of preliminary results of the HQET form factors for the  $B \rightarrow D^{(*)} \ell \nu_\ell$  decays at non-zero recoil have been presented by Fermilab MILC collaboration [31] and JLQCD [32]. The analyses have been done with  $N_f = 2 + 1$  flavors of sea quarks with variable lattice-spacing. They have also done a chiral-continuum-fit to the available lattice points. Though the error budgets are given, it is not complete. To note the impact of these inputs on the SM prediction of  $R(D^*)$ , we have done an analysis only with these inputs; not using experimental data to extract the form-factors. This type of analysis will give us a clear picture of the experimental biases present in the prediction of  $R(D^*)$ , which is important, since we neglect the possibility of new physics effects in  $b \rightarrow c \ell \nu_\ell$  (with  $\ell = \mu$  or  $e$ ) decays in general. Also, using these lattice inputs, we can obtain the decay rate distributions in  $B \rightarrow D^* \ell \nu_\ell$ , which can be compared with the corresponding experimental results. Any discrepancies between the two will lead us to reconsider our understanding.

## II. ANALYSIS WITH THE NEW DATA

### A. Different fits and their comparison

Essentially, there are two form factors  $f_+(z)$  and  $f_0(z)$  relevant for the decays  $B \rightarrow D \ell \nu_\ell$ , while those for the decays  $B \rightarrow D^* \ell \nu_\ell$  are given by  $f(z)$ ,  $g(z)$ ,  $F_1(z)$  and  $F_2(z)$ , respectively. Following the BGL parametrization, each of these form factors can be written as a series expansion in  $z$ ,

$$F_i(z) = \frac{1}{P_i(z)\phi_i(z)} \sum_{n=0}^N a_n^{\mathcal{F}_i} z^n, \quad (2)$$

with

$$z = \frac{\sqrt{w+1} - \sqrt{2}}{\sqrt{w+1} + \sqrt{2}}, \quad (3)$$

where  $w$  is the recoil angle. The mathematical forms of  $\phi_i$ 's and the Blaschke factor  $P_i(z)$  can be seen from [8]. The numerical values of the relevant  $\chi$  functions, associated with the form-factors, are given in table II, with details given in ref. [8, 15]. Here,  $F_i(z)$  include all the relevant form-factors  $f_+(z)$ ,  $f_0(z)$ ,  $F_1(z)$ ,  $f(z)$ ,  $g(z)$  and  $F_2(z)$

$f_+(w)$ & $f_0(w)$	Value from HPQCD	Correlation					
$f_+(1)$	1.178(46)	1.	0.994	0.975	0.507	0.515	0.522
$f_+(1.06)$	1.105(42)		1.	0.993	0.563	0.576	0.587
$f_+(1.12)$	1.037(39)			1.	0.617	0.634	0.649
$f_0(1)$	0.902(41)				1.	0.997	0.988
$f_0(1.06)$	0.870(39)					1.	0.997
$f_0(1.12)$	0.840(37)						1.
Value from MILC							
$f_+(1)$	1.1994(95)	1.	0.967	0.881	0.829	0.853	0.803
$f_+(1.08)$	1.0941(104)		1.	0.952	0.824	0.899	0.886
$f_+(1.16)$	1.0047(123)			1.	0.789	0.890	0.953
$f_0(1)$	0.9026(72)				1.	0.965	0.868
$f_0(1.08)$	0.8609(77)					1.	0.952
$f_0(1.16)$	0.8254(94)						1.

TABLE I: Lattice QCD results of  $f_+$  and  $f_0$  for different values of  $w$ . The upper half of the table have been obtained using the fit results from the HPQCD collaboration [6], and the lower half are the results obtained by the Fermilab MILC collaboration [5].

$\chi_{0+}^L(0) = 6.204 \times 10^{-3}$
$\tilde{\chi}_{0-}^L(0) = 19.421 \times 10^{-3}$
$\tilde{\chi}_{1-}^T(0) = 5.131 \times 10^{-4} GeV^{-2}$
$\chi_{1+}^T(0) = 3.894 \times 10^{-4} GeV^{-2}$

TABLE II: Various inputs in our analysis, the  $\chi$ 's are the functions relevant for BGL parametrizations of the formfactors, for detail see [8, 14]

respectively. The coefficients  $a_n^{\mathcal{F}_i}$  obey both weak and strong unitarity constraints. Here,  $z$  is a kinematic variable and for the semileptonic decays under consideration, its values lie between 0 and 0.0456; for details, see [8]. The form factors in the decays  $B \rightarrow D\ell\nu_\ell$  and  $B \rightarrow D^*\ell\nu_\ell$  can be fully expressed in terms of heavy quark effective theory (HQET) form-factors  $h_V(w), h_{A_1}(w), h_{A_2}(w)$  and  $h_{A_3}(w)$ . As mentioned earlier, we have simultaneously extracted  $|V_{cb}|$  and the form-factors  $f(z), F_1(z)$ , and  $g(z)$  from the fit to the available new data on the differential rates and angular distributions in  $B \rightarrow D^*\ell\nu_\ell$  [17] (and using the lattice input on the form factor  $h_{A_1}(1) = 0.906(13)$  from the unquenched Fermilab/MILC lattice data [4]). Using these fit results and the inputs given in table I, we have predicted  $R(D^*)$ , and other relevant observables like the tau-polarization  $P_\tau(D^*)$ ,  $D^*$ -polarization  $F_L(D^*)$ , and the forward-backward asymmetry  $A_{FB}(D^*)$ . Since there are no new updates on  $B \rightarrow D\ell\nu_\ell$  decay, we do not repeat the analysis of this decay mode.

As mentioned earlier, we have analyzed the data using different orders of truncation in the series expansion of the form-factors and compared them. Though our main focus is on the BGL form-factors which are truncated at  $N = 2$ , i.e.,  $(n_f, n_{F_1}, n_g) \equiv (2, 2, 2)$ , we perform several other  $\chi^2$  fits by varying the order of truncation of each of the BGL form factors from 0 to 2 independently to study their sensitivity to the present data. We have considered all possible combinations of the values of  $n_f, n_{F_1}$  and  $n_g$  ranging between 0 and 2. We then use the second-order variant of Akaike's Information Criterion ( $AIC_c$ ) to do a data-based comparison and ranking of all the scenarios in hand. We would like to point out here that we have used weak unitarity bounds as constraints in all these fits, which have been neglected in ref. [21]. We find that the combination  $(n_f, n_{F_1}, n_g) \equiv (1, 2, 0)$  forms the best scenario to explain the present Belle data. We then perform Bayesian fits for this best case, as well as for  $N = 2$  and the fit results for  $B \rightarrow D^*\ell\nu_\ell$  form factor parameters are given in Table III. We have made the necessary corrections to avoid the bias due to the D'Agostini effect [18] while using the experimental systematic uncertainties in these Bayesian fits. The second column lists the fit results for the scenario  $(1, 2, 0)$  while the third column contains the fit results for  $(2, 2, 2)$ . As

Parameters	$n_f = 1, n_{F_1} = 2, n_g = 0$	$n_f = n_{F_1} = n_g = N = 2$	
	Belle 2019 data +	Belle 2019 data +	Belle 2019 data + LCSR at $q^2 = 0$ [20]
	$h_{A_1}(1)$ from MILC [4]	$h_{A_1}(1)$ from MILC [4]	+ $h_{A_1}(1)$ from MILC [4]
$ V_{cb}  \times 10^3$	39.76 ( $\frac{87}{98}$ )	39.37 ( $\frac{1.07}{1.21}$ )	39.56 ( $\frac{1.04}{1.06}$ )
$a_0^f$	0.0122(2)	0.0122(2)	0.0122(2)
$a_1^f$	0.0056 ( $\frac{54}{58}$ )	0.0012 ( $\frac{171}{286}$ )	0.0256 ( $\frac{232}{168}$ )
$a_2^f$	–	0.0792(5474)	–0.3108(4175)
$a_1^{\mathcal{F}1}$	0.0062 ( $\frac{20}{21}$ )	0.0068 ( $\frac{22}{24}$ )	0.0063 ( $\frac{21}{19}$ )
$a_2^{\mathcal{F}1}$	-0.1128 ( $\frac{333}{352}$ )	-0.1157 ( $\frac{412}{392}$ )	-0.1033 ( $\frac{323}{366}$ )
$a_0^g$	0.0268 ( $\frac{7}{8}$ )	0.0289 ( $\frac{81}{126}$ )	0.0272 ( $\frac{42}{47}$ )
$a_1^g$	–	-0.0840 ( $\frac{1812}{1343}$ )	-0.0088 ( $\frac{1199}{1031}$ )
$a_2^g$	–	-0.0016(5304)	0.0013(5699)

TABLE III: The results of the fit to new Belle data [17] in  $B \rightarrow D^* \ell \nu_\ell$  decay using BGL parametrization of the form factors for  $n_f = 1, n_{F_1} = 2, n_g = 0$  (second column) and for  $N = 2$  (third column). The last (fourth) column corresponds to the fit to new Belle data [17] together with LCSR inputs (for  $q^2 = 0$ ) [20] for  $N = 2$ .

expected, the extracted parameters in the best possible scenario have smaller uncertainties compared to those in the scenario (2, 2, 2). Also, the coefficients/parameters of the expansion which are dropped in (1, 2, 0)-scenario have large uncertainties in the scenario (2, 2, 2), which points to the fact that the present data is not sensitive enough to extract the higher powers of the expansion. The probability distributions for the BGL coefficients of all the  $B \rightarrow D^* \ell \nu_\ell$  form factors corresponding to the  $N = 2$  Bayesian fit and the correlations between them are depicted in Figure 1. We note that the posterior distributions of the second-order coefficients of the BGL expansion are almost flat: indicative of the poor sensitivities of these coefficients toward the present data.

Very recently, there are updates from LCSR on the form-factors  $V(q^2), A_1(q^2), A_2(q^2)$  and  $A_0(q^2)$  at  $q^2 = 0$  [20]. These QCD form-factors can be expressed in terms of the BGL form-factors,  $g, f, F_1$  and  $F_2$ . We have utilized these newly available LCSR results along with the other inputs and performed a Bayesian fit. The results are presented in the fourth column of table III. The LCSR inputs are also available for a few other values of  $q^2 = -5, -10, -15$  (in  $GeV^2$ ). However, we have not used these inputs in our analysis because of the reason stated in the following. The BGL parametrization of the form-factors rely on a Taylor series expansion about  $z = 0$ . The key ingredient in this approach is the transformation that maps the complex  $q^2$  plane onto the unit disc  $|z| \leq 1$ . Therefore, small values of  $z$  ensure faster convergence of the series. Now, for the semileptonic decay  $B \rightarrow D^* \ell \nu$ , the kinematically allowed region is  $0 < z \leq 0.0456$ . In this semileptonic region, the maximum value of  $z$  is obtained at  $q^2 = 0(GeV^2)$ , and thus the large negative values of  $q^2$  lead to a value of  $z$  which is very close to 1. Hence, we mostly concentrate on the LCSR inputs for  $q^2 = 0$  for the BGL form factor fits. The extracted  $|V_{cb}|$  is consistent with the one obtained without LCSR inputs.

The  $w$ -distributions of the form-factors in  $B \rightarrow D^* \ell \nu_\ell$ , extracted from different fits in table III, are shown in figure 2. It compares the  $w$  dependence of the three  $B \rightarrow D^* \ell \nu_\ell$  form factors,  $f(w), F_1(w)$  and  $g(w)$  obtained from three different Bayesian fits. The effects of the choices of experimental and theory inputs and the order of truncation of BGL expansion can be seen in these figures. There are differences between the results obtained using the 2017 [7] and the 2019 Belle results [17], for all the form-factors. These differences become more prominent in the large-recoil limit, since the lattice results play an important role in constraining the BGL coefficients in the zero-recoil. Also, the  $w$ -dependence of the respective form-factors are consistent with each other for both the scenarios (1, 2, 0) and (2, 2, 2). As expected, the errors are a little less in the scenario (1, 2, 0). The  $w$ -dependence of all the form-factors are unaltered after incorporating the inputs from LCSR at maximum recoil, with the respective uncertainties reduced.

## B. $R(D^*)$ in the SM

We also obtain estimates for  $R(D^*)$  and other  $B \rightarrow D^* \tau \nu_\tau$  observables for all the fits; as listed in table III for  $N = 2$ . As mentioned earlier, there will be one additional form-factor  $F_2(z)$  in  $B \rightarrow D^* \tau \nu_\tau$ , which we can not constrain from the experimental data in  $B \rightarrow D^* \ell \nu_\ell$ . We estimate the parameters of  $F_2(z)$  by exploiting the HQET relations between the form-factors as shown in our earlier work [15]. In the following, we will briefly describe the method; for more details, see [15].

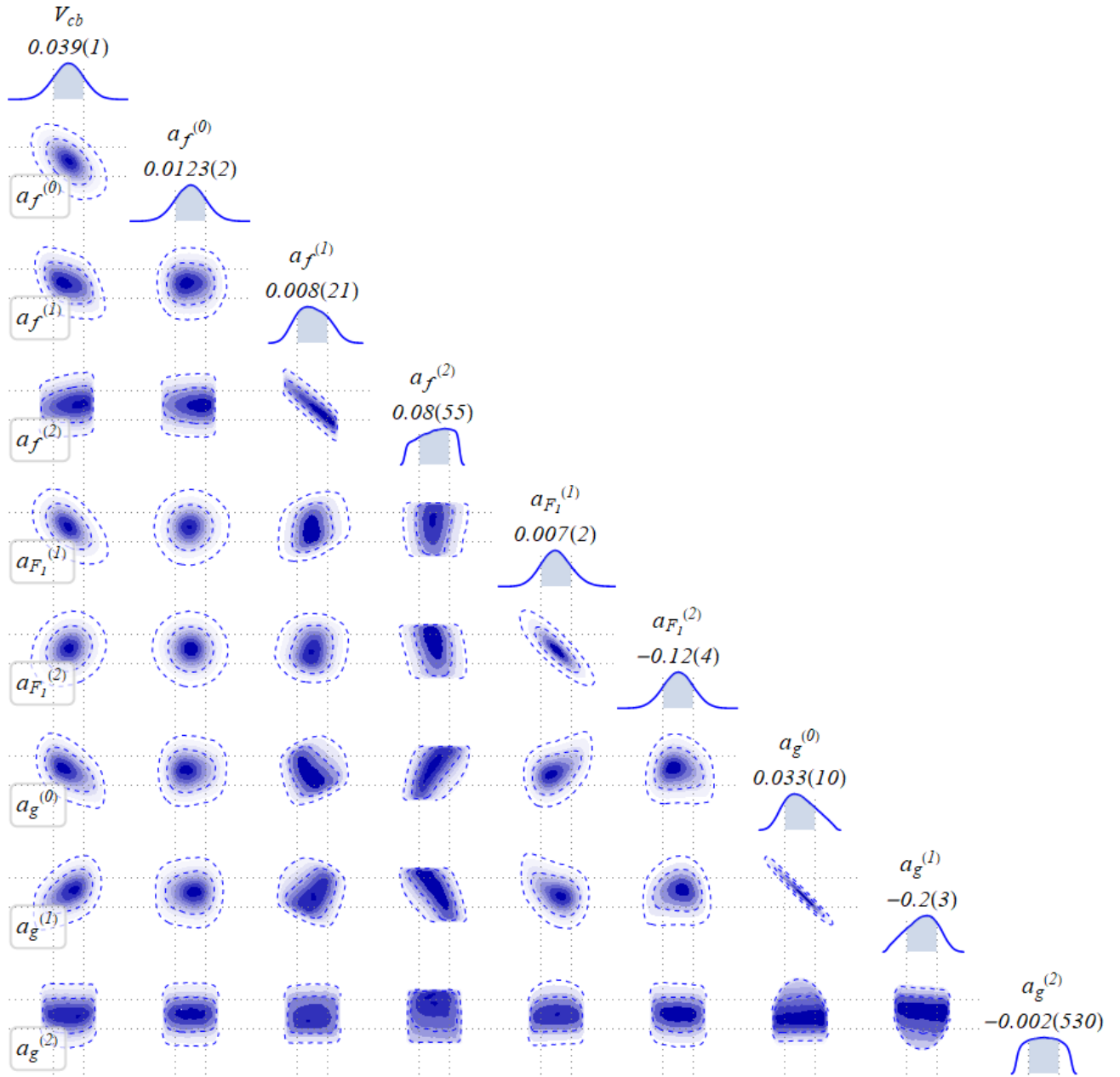


FIG. 1: The probability distributions from the Bayesian fit to all the BGL parameters of  $B \rightarrow D^* \ell \nu_\ell$  form factors corresponding to  $N = 2$  and the correlations between them

Parameters	$\eta(1)$	$\eta'(1)$	$\chi_2(1)$	$\chi_2'(1)$	$\chi_3'(1)$	$\Delta_{\mp}$
Values	0.373 ( $\frac{89}{58}$ )	-0.060 ( $\frac{41}{33}$ )	-0.059(20)	-0.003 ( $\frac{19}{21}$ )	0.037 ( $\frac{18}{19}$ )	0.91(21)

TABLE IV: The fit results for the sub-leading Isgur-Wise functions and  $\Delta_{\mp}$

The ratio  $f_+(w)/f_0(w)$  can be expressed in HQET up to order  $\mathcal{O}(\alpha_S)$  in perturbative corrections and  $\mathcal{O}(\Lambda_{QCD}/m_{b,c})$  in non-perturbative corrections [9, 13], which are expressed in terms of a few sub-leading Isgur-Wise functions:  $\eta(1)$ ,  $\eta'(1)$ ,  $\chi_2(1)$ ,  $\chi_2'(1)$ , and  $\chi_3'(1)$ . We use the lattice inputs on  $B \rightarrow D\ell\nu_\ell$  (table I) to create synthetic data-points for the HQET fit to the sub-leading Isgur-Wise functions. For example, we consider the ratio  $f_+(w)/f_0(w)$  for  $w = 1, 1.08, 1.16$ , using lattice data from MILC and for  $w = 1, 1.03, 1.06, 1.09, 1.12$ , using lattice data from HPQCD.

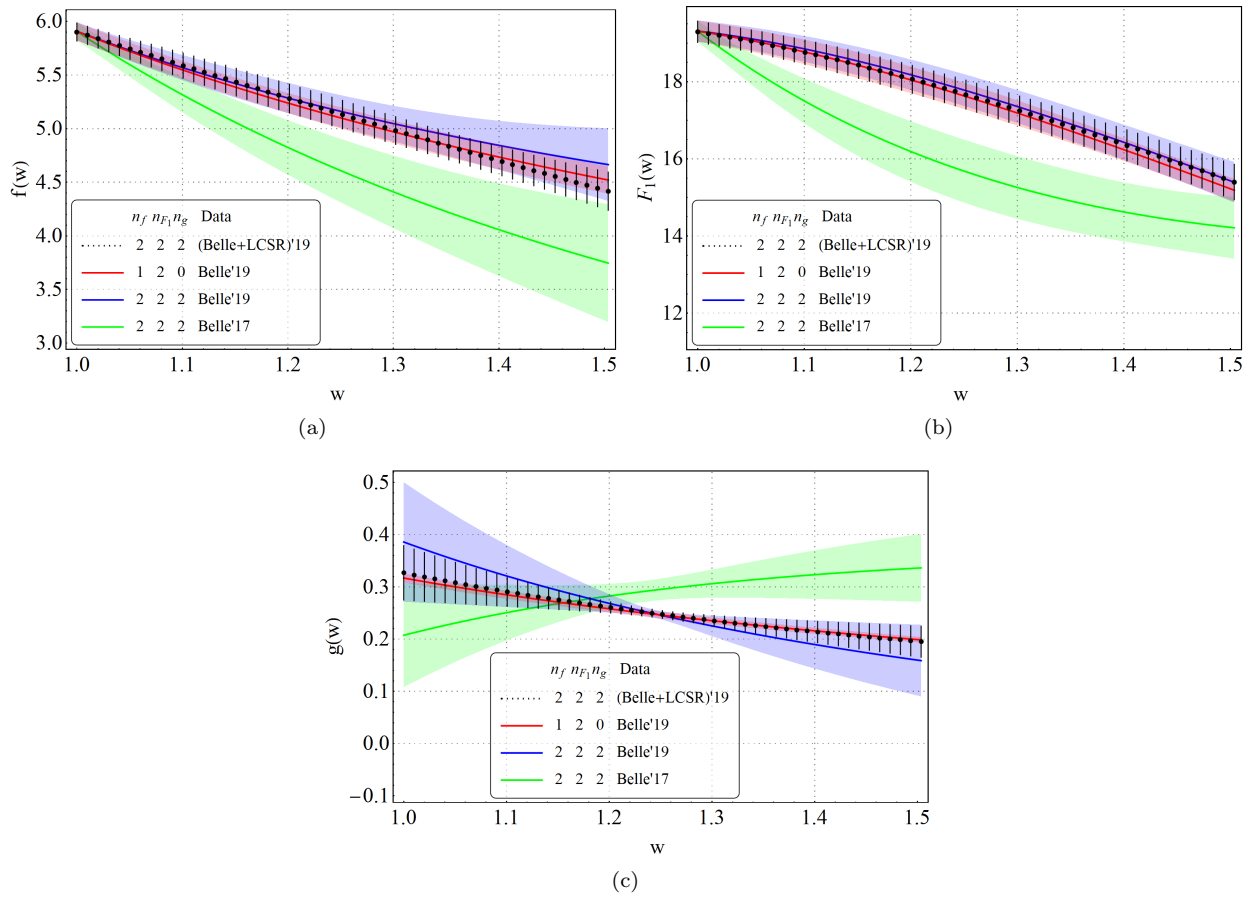


FIG. 2: Comparison between the shape of  $B \rightarrow D^* \ell \nu_\ell$  form factors obtained from the  $B \rightarrow D^* \ell \nu_\ell$  fit using BGL parametrization to old Belle data (green band) for  $N=2$ , to new Belle data for  $N=2$  (blue band), to new Belle data for  $n_f = 1, n_{F_1} = 2, n_g = 0$  (red band), and to new Belle data together with LCSR inputs [20] (black bars).

Other relevant inputs like the quark masses ( $m_b, m_c$ ),  $\alpha_S$  and  $\Lambda_{QCD}$  are taken from the reference [13]. We use these eight synthetic data-points to perform a Bayesian fit to the sub-leading Isgur-Wise functions  $\eta(1)$ ,  $\eta'(1)$ ,  $\chi_2(1)$ ,  $\chi_2'(1)$ , and  $\chi_3'(1)$ . We observe that  $\chi_2(1)$ ,  $\chi_2'(1)$ , and  $\chi_3'(1)$  are relatively insensitive to the form factor ratios used in the fit and hence, we use the QCDSR predictions [13] for  $\chi_2(1)$ ,  $\chi_2'(1)$ , and  $\chi_3'(1)$  to specify the prior distributions for these parameters in the Bayesian fit.

In addition, to account for the missing higher order corrections, several normalizing parameters ( $\Delta$ s) have been introduced here in the ratios of the HQET form factors. We just need to make the following replacements in order to be able to estimate the size of these higher order corrections:

$$\frac{h_v}{h_{A_1}} \rightarrow \frac{h_v}{h_{A_1}} \Delta_v, \quad \frac{h_{A_3}}{h_{A_1}} \rightarrow \frac{h_{A_3}}{h_{A_1}} \Delta_{31}, \quad \frac{h_{A_2}}{h_{A_1}} \rightarrow \frac{h_{A_2}}{h_{A_1}} \Delta_{21}, \quad \frac{h_-}{h_+} \rightarrow \frac{h_-}{h_+} \Delta_{\mp}, \quad \frac{h_+}{h_{A_1}} \rightarrow \frac{h_+}{h_{A_1}} \Delta. \quad (4)$$

For the ratio  $f_+(w)/f_0(w)$ , the only normalizing parameter involved is  $\Delta_{\mp}$ . We use the conservative estimate for  $\Delta_{\mp} = 1 \pm 0.2$  to define its prior distribution in the Bayesian fit. The fit results for the sub-leading Isgur-Wise functions and  $\Delta_{\mp}$  are summarized in table IV.

Finally, using the following equation:

$$\left( \frac{F_2(w)}{f_+(w)} \right)_{BGL} = \left( \frac{F_2(w)}{f_+(w)} \right)_{HQET}, \quad (5)$$

we express  $F_2(w)/f_{+,0}(w)$  in terms of the sub-leading Isgur-Wise functions. We have created synthetic data points for the right hand side of the above equation using the fit results given in table IV. Three more normalizing parameters,  $\Delta_{21}$ ,  $\Delta_{31}$  and  $\Delta$ , come into play here in defining these ratios and we use their conservative estimates:  $\Delta_{21} = 1 \pm 0.2$ ,  $\Delta_{31} = 1 \pm 0.2$ , and  $\Delta = 1 \pm 0.1$ . As the BGL coefficients for the form factors  $f_+$  and  $f_0$  are already known from the

Inputs used in the fit	Belle 2017 [7] +				Belle 2019 [17] +				Belle 2019 [17]+LCSR at $q^2 = 0$ [20],			
	$h_{A_1}(1)$ from MILC [4]				$h_{A_1}(1)$ from MILC [4]				$h_{A_1}(1)$ from MILC [4]			
Observable	$R(D^*)$	$P_\tau^{(D^*)}$	$F_L^{D^*}$	$A_{FB}^{(D^*)}$	$R(D^*)$	$P_\tau^{(D^*)}$	$F_L^{D^*}$	$A_{FB}^{(D^*)}$	$R(D^*)$	$P_\tau^{(D^*)}$	$F_L^{D^*}$	$A_{FB}^{(D^*)}$
Value	0.256	-0.485	0.458	-0.033	0.251	-0.492	0.469	-0.038	0.252	-0.490	0.469	-0.026
Error	$(+0.007)$ $(-0.008)$	$(+0.026)$ $(-0.028)$	$(+0.015)$ $(-0.017)$	0.024	$(+0.004)$ $(-0.005)$	$(+0.025)$ $(-0.024)$	$(+0.010)$ $(-0.011)$	$(+0.022)$ $(-0.021)$	$(+0.006)$ $(-0.007)$	$(+0.032)$ $(-0.036)$	$(+0.014)$ $(-0.015)$	0.020
Correlation Matrix	1	0.639	0.448	0.354	1	0.944	0.839	0.617	1	0.978	0.942	0.886
		1	0.596	0.554		1	0.830	0.572		1	0.944	0.886
			1	0.742			1	0.764			1	0.921
				1				1				1

TABLE V: SM predictions and the correlations for the observables in  $B \rightarrow D^* \tau \nu_\tau$  decays. The estimates corresponding to the 2017 Belle data correspond to the analysis in our earlier work [15]

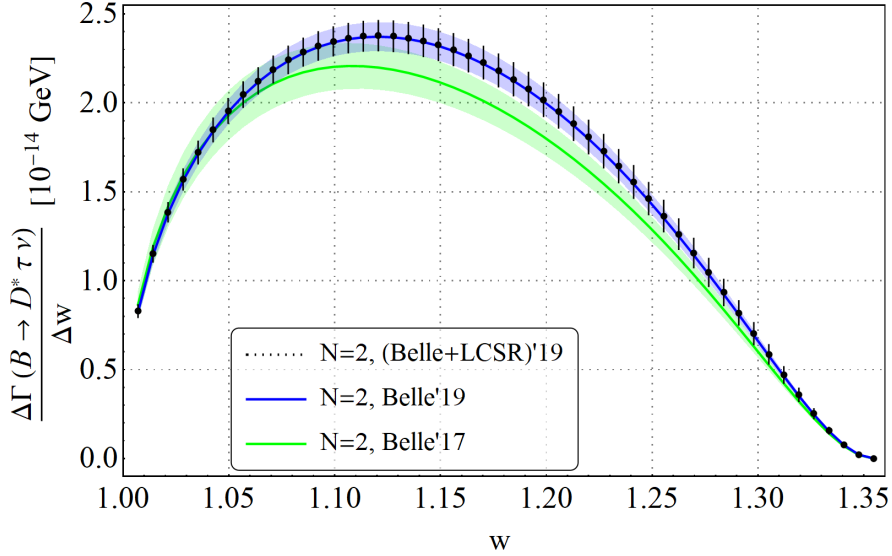


FIG. 3: Comparison between  $B \rightarrow D^* \tau \nu_\tau$  decay distributions obtained from different fit scenarios given in table V.

$B \rightarrow D \ell \nu_\ell$  fit [15], the only unknowns are the BGL coefficients of  $F_2$  for  $N = 2$ , i.e.  $a_0^{\mathcal{F}_2}$ ,  $a_1^{\mathcal{F}_2}$ , and  $a_2^{\mathcal{F}_2}$ . We use the QCD relation  $A_0(q^2 = 0) = A_3(q^2 = 0)$ , which is equivalent to

$$F_2(q^2 = 0) = \frac{2F_1(q^2 = 0)}{m_B^2 - m_{D^*}^2}, \quad (6)$$

to eliminate  $a_1^{\mathcal{F}_2}$  (for details, see [15]). Thus, in an attempt to obtain a conservative estimate of the form factor  $F_2$ , we fit the BGL parameters  $a_0^{\mathcal{F}_2}$  and  $a_2^{\mathcal{F}_2}$  to the above-generated synthetic data-points.

In this fit, we use the weak unitarity constraints for the BGL coefficients. As we find that this Bayesian fit is highly insensitive to the BGL coefficient  $a_2^{\mathcal{F}_2}$ , we have set  $a_2^{\mathcal{F}_2} = 0$  without any loss of generality in making the predictions of the  $B \rightarrow D^* \tau \nu_\tau$  observables. Using the estimate of  $a_0^{\mathcal{F}_2}$  together with the fit results for the BGL  $B \rightarrow D^* \ell \nu_\ell$  form factor coefficients for  $N = 2$ , we have estimated  $R(D^*)$ ,  $P_\tau(D^*)$ ,  $F_L(D^*)$ , and  $A_{FB}(D^*)$ , which are tabulated in table V. Note that the prediction for  $P_\tau(D^*)$  is consistent with measurement [33]. On the other hand,  $F_L^{D^*}$  is only consistent with the corresponding measurement [34] at  $2\sigma$ . Also, the SM prediction is lower than the experimental result. For the detailed mathematical expressions of these angular observables, see [35]. The estimates are given only for the analysis with the BGL coefficients at order  $N = 2$ . The second and third column of the table V shows the predictions for the same observables using Belle 2017 and Belle 2019 data, respectively. We note that all the predicted values are consistent with each other within the error-bars. While we note a reduction in uncertainty in all the observables for the present data set, the central value of  $R(D^*)$  has reduced by  $\approx 2\%$ . The fourth/last column represents the results which are obtained using the fit results with LCSR inputs at  $q^2 = 0$ . Here, we extract  $a_0^{\mathcal{F}_2}$  as before, but  $a_1^{\mathcal{F}_2}$  is

constrained using the LCSR input  $A_0(q^2 = 0) = 0.68 \pm 0.18$ <sup>1</sup>, not from the equation 6. Therefore,  $F_2(z)$ , in this case, is extracted using only the theory inputs like lattice and LCSR, without any impact from the experimental inputs on  $B \rightarrow D^* \ell \nu_\ell$ . This is why all the predictions have large errors, though they are consistent with the predictions given in second and third columns of the same table. Figure 3 compares the  $B \rightarrow D^* \tau \nu_\tau$  decay distributions for the scenarios discussed in table V. We can see that the black bars and the blue bands are consistent within error bars as both the scenarios depend on exactly the same experimental inputs for the Bayesian fits. However, the results obtained using Belle 2017 data differ from these new results, as seen before.

### III. NEW PHYSICS ANALYSIS

Experiment	Observable	Value
BaBar	$R(D)$	$0.440 \pm 0.058 \pm 0.042$
[36]	$R(D^*)$	$0.332 \pm 0.024 \pm 0.018$
Belle(2015)	$R(D)$	$0.375 \pm 0.064 \pm 0.026$
[37]	$R(D^*)$	$0.293 \pm 0.038 \pm 0.015$
LHCb(2015) [38]	$R(D^*)$	$0.336 \pm 0.027 \pm 0.030$
Belle(2017)	$R(D^*)$	$0.270 \pm 0.035 \left( \begin{smallmatrix} +0.028 \\ -0.025 \end{smallmatrix} \right)$
[33]	$P_\tau(D^*)$	$-0.38 \pm 0.51 \left( \begin{smallmatrix} +0.21 \\ -0.16 \end{smallmatrix} \right)$
LHCb(2017) [39]	$R(D^*)$	$0.291 \pm 0.019 \pm 0.026 \pm 0.013$
Belle(2019) [34]	$F_L(D^*)$	$0.60 \pm 0.08 \pm 0.04$
Belle(2019)	$R(D)$	$0.307 \pm 0.037 \pm 0.016$
[40, 41]	$R(D^*)$	$0.283 \pm 0.018 \pm 0.014$
World averages	$R(D)$	$0.340 \pm 0.027 \pm 0.013$
	$R(D^*)$	$0.295 \pm 0.011 \pm 0.008$

TABLE VI: Experiment inputs for  $R(D^{(*)})$ ,  $P_\tau(D^*)$  and  $F_L(D^*)$  used in the New Physics fits.

The SM predictions given in table V can be compared with the respective measurements given in table VI. We note that there still are discrepancies in the data on  $R(D^*)$ . Our predictions of  $R(D^*)$  in the analysis with Belle 2018 data sets (without LCSR) are consistent with the respective world average at  $\sim 3\sigma$ , while being consistent with the most recent results by Belle (2019) at  $\sim 1.5\sigma$ . On the other hand, our predictions, with LCSR as inputs, are consistent with the world average at  $\sim 3\sigma$  and with the most recent result of Belle (2019) at  $\sim 1.5\sigma$ . Also, the predictions of  $R(D)$  [16] are consistent with the respective world average at  $\sim 3\sigma$ . All these observations taken together could be indicating to the presence of a non-zero new physics. In this section, we will constrain possible NP scenarios from the data in a model independent way.

The most general effective Hamiltonian describing the  $b \rightarrow c \tau \nu_\tau$  transitions is given by

$$\mathcal{H}_{eff} = \frac{4G_F}{\sqrt{2}} V_{cb} [(\delta_{\ell\tau} + C_{V_1}^\ell) \mathcal{O}_{V_1}^\ell + C_{V_2}^\ell \mathcal{O}_{V_2}^\ell + C_{S_1}^\ell \mathcal{O}_{S_1}^\ell + C_{S_2}^\ell \mathcal{O}_{S_2}^\ell + C_T^\ell \mathcal{O}_T^\ell], \quad (7)$$

where  $\mathcal{O}_W^\ell$  ( $W = V_1, V_2, S_1, S_2, T$ ) are the Wilson coefficients (WCs) corresponding to the following four-Fermi operators:

$$\begin{aligned} \mathcal{O}_{V_1}^\ell &= (\bar{c}_L \gamma^\mu b_L)(\bar{\tau}_L \gamma_\mu \nu_{\ell L}), & \mathcal{O}_{V_2}^\ell &= (\bar{c}_R \gamma^\mu b_R)(\bar{\tau}_L \gamma_\mu \nu_{\ell L}), & \mathcal{O}_{S_1}^\ell &= (\bar{c}_L b_R)(\bar{\tau}_R \nu_{\ell L}), \\ \mathcal{O}_{S_2}^\ell &= (\bar{c}_R b_L)(\bar{\tau}_R \nu_{\ell L}), & \mathcal{O}_T^\ell &= (\bar{c}_R \sigma^{\mu\nu} b_L)(\bar{\tau}_R \sigma_{\mu\nu} \nu_{\ell L}). \end{aligned} \quad (8)$$

<sup>1</sup> This numerical value has been obtained using the values of  $A_1(0)$  and  $A_2(0)$  from [20].

Case	New WCs	$R(D)$	$R(D^*)$	$\mathcal{B}(B_c \rightarrow \tau\nu_\tau)$	Allowed or not? (Remarks)
1	$\mathcal{Re}[C_{V_1}]$	0.350( $\frac{11}{13}$ )	0.293 (10)	0.024(2)	Yes
2	$\mathcal{Re}[C_{V_2}]$	0.256(16)	0.294 ( $\frac{14}{13}$ )	0.024(2)	Yes ( $R(D)$ at $2\sigma$ )
3	$\mathcal{Re}[C_{S_1}]$	0.377 ( $\frac{23}{25}$ )	0.262 ( $\frac{5}{6}$ )	0.049(12)	Yes ( $R(D^*)$ at $2\sigma$ )
4	$\mathcal{Re}[C_{S_2}]$	0.324 ( $\frac{26}{28}$ )	0.306(10)	0.877(92)	No
5	$\mathcal{Re}[C_T]$	0.293(4)	0.303 ( $\frac{13}{13}$ )	0.020(2)	Yes ( $R(D)$ at $2\sigma$ )
6	$\mathcal{Re}[C_{V_1}]$ , $\mathcal{Im}[C_{V_1}]$	0.351 ( $\frac{13}{12}$ )	0.294 ( $\frac{10}{9}$ )	0.024(2)	Yes
7	$\mathcal{Re}[C_{V_2}]$ , $\mathcal{Im}[C_{V_2}]$	0.334 ( $\frac{32}{28}$ )	0.298 ( $\frac{13}{14}$ )	0.024(3)	Yes
8	$\mathcal{Re}[C_{S_1}]$ , $\mathcal{Im}[C_{S_1}]$	0.380 ( $\frac{23}{25}$ )	0.261(6)	0.057 (26)	Yes ( $R(D^*)$ at $2\sigma$ )
9	$\mathcal{Re}[C_{S_2}]$ , $\mathcal{Im}[C_{S_2}]$	0.337 ( $\frac{28}{26}$ )	0.299(11)	0.823 (107)	No
10	$\mathcal{Re}[C_T]$ , $\mathcal{Im}[C_T]$	0.296 ( $\frac{7}{17}$ )	0.301(13)	0.020(2)	Yes
11	$\mathcal{Re}[C_{V_1}]$ , $\mathcal{Re}[C_{V_2}]$	0.337 ( $\frac{31}{30}$ )	0.298 ( $\frac{12}{13}$ )	0.024(3)	Yes
12	$\mathcal{Re}[C_{S_1}]$ , $\mathcal{Re}[C_{S_2}]$	0.333 ( $\frac{29}{32}$ )	0.299(13)	0.534 (224)	Marginally (see fig. 5g)

TABLE VII:  $R(D^{(*)})$  predictions for the different New Physics scenarios using the fit to all the experimental inputs. The cases with  $\mathcal{B}(B_c \rightarrow \tau\nu_\tau) > 30\%$  are physically ruled out

Case	New WCs	$R(D)$	$R(D^*)$	$\mathcal{B}(B_c \rightarrow \tau\nu_\tau)$	Allowed or not? (Remarks)
1	$\mathcal{Re}[C_{V_1}]$	0.339(13)	0.284(10)	0.023(2)	Yes
2	$\mathcal{Re}[C_{V_2}]$	0.261( $\frac{17}{18}$ )	0.288 ( $\frac{16}{15}$ )	0.023(3)	Yes ( $R(D)$ at $2\sigma$ )
3	$\mathcal{Re}[C_{S_1}]$	0.355 ( $\frac{26}{27}$ )	0.259 ( $\frac{5}{6}$ )	0.039 (12)	Yes ( $R(D^*)$ at $2\sigma$ )
4	$\mathcal{Re}[C_{S_2}]$	0.301(30)	0.302(10)	0.826(95)	No
5	$\mathcal{Re}[C_T]$	0.294(4)	0.292 ( $\frac{14}{15}$ )	0.020(2)	Yes ( $R(D)$ at $2\sigma$ )
6	$\mathcal{Re}[C_{V_1}]$ , $\mathcal{Im}[C_{V_1}]$	0.339 ( $\frac{14}{13}$ )	0.285 ( $\frac{12}{9}$ )	0.023(2)	Yes
7	$\mathcal{Re}[C_{V_2}]$ , $\mathcal{Im}[C_{V_2}]$	0.307 ( $\frac{30}{32}$ )	0.292 ( $\frac{15}{14}$ )	0.024(3)	Yes
8	$\mathcal{Re}[C_{S_1}]$ , $\mathcal{Im}[C_{S_1}]$	0.357 ( $\frac{25}{28}$ )	0.257(6)	0.049(33)	Yes ( $R(D^*)$ at $2\sigma$ )
9	$\mathcal{Re}[C_{S_2}]$ , $\mathcal{Im}[C_{S_2}]$	0.316 ( $\frac{31}{29}$ )	0.294(13)	0.755(71)	No
10	$\mathcal{Re}[C_T]$ , $\mathcal{Im}[C_T]$	0.298 ( $\frac{7}{12}$ )	0.292 ( $\frac{15}{13}$ )	0.020(2)	Yes
11	$\mathcal{Re}[C_{V_1}]$ , $\mathcal{Re}[C_{V_2}]$	0.318 ( $\frac{31}{29}$ )	0.291 ( $\frac{15}{14}$ )	0.024(3)	Yes
12	$\mathcal{Re}[C_{S_1}]$ , $\mathcal{Re}[C_{S_2}]$	0.316 ( $\frac{31}{29}$ )	0.292(14)	0.409(228)	Marginally (see fig. 5g)

TABLE VIII:  $R(D^{(*)})$  predictions for the different New Physics scenarios using the fit to all the experimental inputs except the ones from BaBar. The cases with  $\mathcal{B}(B_c \rightarrow \tau\nu_\tau) > 30\%$  are physically ruled out

Here, we have considered only the left handed neutrinos.

We fit these Wilson coefficients to the available data on the integrated observables in  $B \rightarrow D^* \tau \nu_\tau$  decay from BaBar, Belle and LHCb collaborations in order to estimate the size of the different NP effects allowed by the present experimental scenario. All the different experimental inputs to this NP fit are listed in the table VI. Detailed expressions for the observables  $R(D^*)$ ,  $P_\tau(D^*)$ ,  $F_L(D^*)$ , and  $\mathcal{B}(B_c \rightarrow \tau\nu_\tau)$  in terms of the WCs can be found in the references [35, 42]. We consider several simple NP scenarios with both real and complex WCs, with a maximum of two NP fit parameters at a time, the respective cases are listed in tables VII and VIII. In these Bayesian fits, the results from the analysis in Section II (corresponding to second column of table V) are used to define the prior distributions for the BGL coefficients corresponding to ( $N = 2$ ) for all the  $B \rightarrow D^* \ell \nu_\ell$  form factors while for the prior distributions for  $B \rightarrow D$  form-factors, we depend on the  $B \rightarrow D \ell \nu_\ell$  analysis in our earlier work [15].

Table VII gives the predictions of  $R(D^{(*)})$  in different NP scenarios which are obtained from a fit to all the experimental inputs while table VIII lists the  $R(D^{(*)})$  predictions corresponding to the fit after dropping the experimental input from BaBar. As was already pointed out in reference [42], the cases with  $\mathcal{B}(B_c \rightarrow \tau\nu_\tau) > 30\%$  are physically ruled out. In the SM we get a prediction for  $\mathcal{B}(B_c \rightarrow \tau\nu_\tau) = 0.020 \pm 0.002$ . The tensor operators do not contribute to

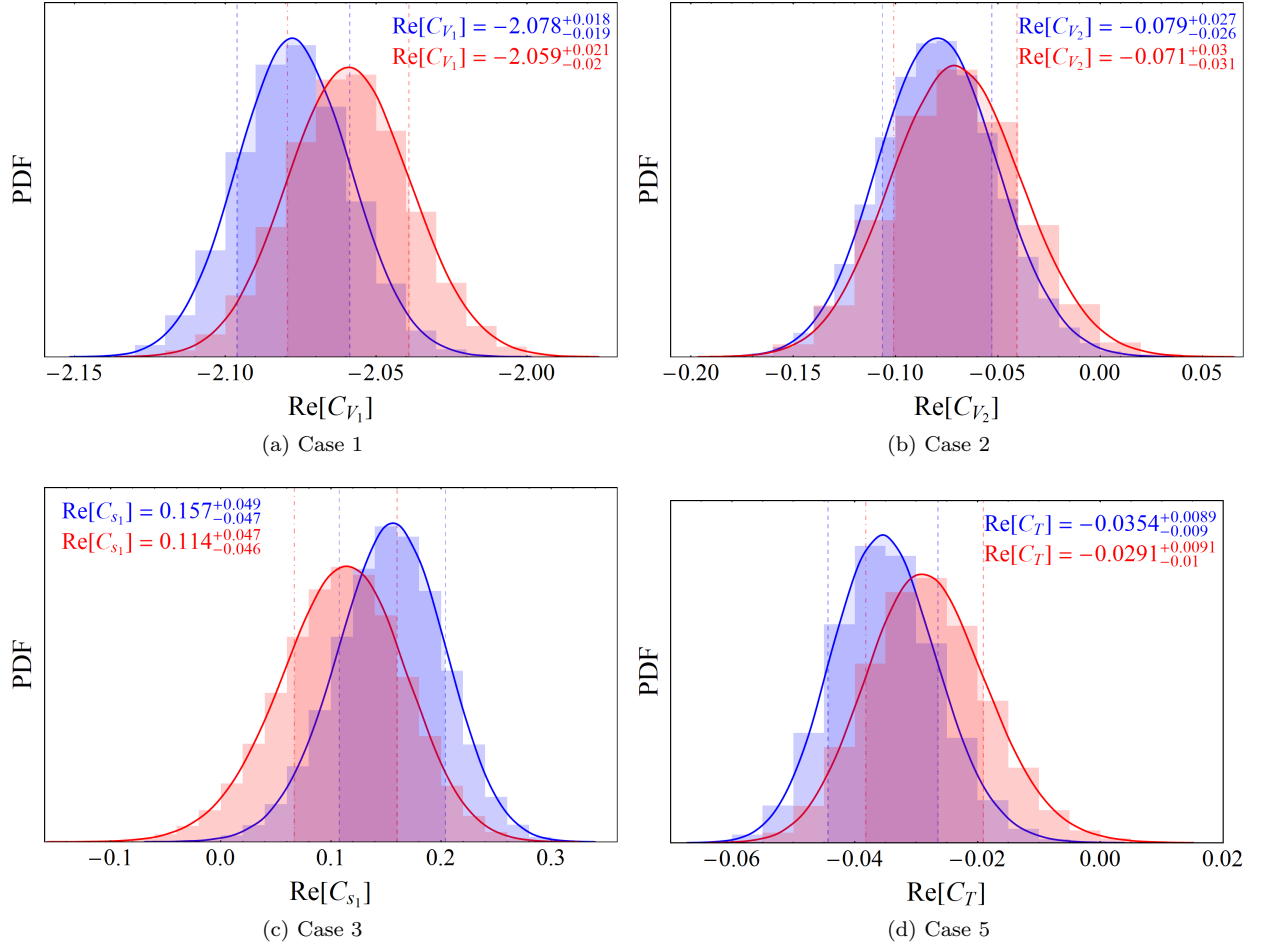


FIG. 4: Posterior distributions of the new WCs in the allowed one parameter New Physics scenarios in tables VII and VIII. The blue histograms correspond to the New Physics fits to all the experimental inputs in table VI while the red histograms correspond to the fits to all experimental inputs except BaBar. The blue dashed lines and the red dot-dashed lines represent the 68% credible intervals (high density region around mode) for the respective posterior distributions.

the transition  $B_c \rightarrow \tau\nu_\tau$ , and hence the NP parameter space for the WC  $\mathcal{O}_T^\ell$  cannot be constrained by the bounds on  $\mathcal{B}(B_c \rightarrow \tau\nu_\tau)$ . We note that apart from the scenario with the WC  $C_{S_2}$  (both real and complex), all other scenarios are favored (strongly, more or less) by the present data. Among the most favored NP scenarios, there are SM type new four-fermion operators ( $\mathcal{O}_{V_1}$ ) with real or complex WCs.

Posterior distributions of the WCs in all the allowed one parameter scenarios are shown in figure 4 with the  $1\sigma$  Credible Intervals (CI) around the central moment of the relevant WCs mentioned. The blue shaded regions correspond to the NP fits to all the experimental inputs in table VI, while the red shaded ones correspond to those with the experimental inputs from BaBar dropped. Note that, in some cases, there are slight changes in the allowed regions after dropping the BaBar data. For the two-parameter scenarios, we have shown the correlations between the WCs for the allowed NP scenarios in figures 5 and 6. The solid and the dashed contours enclose the 68% and 95% probability regions, respectively. The gray shaded region in the figures depict the NP parameter space disallowed by the constraint  $\mathcal{B}(B_c \rightarrow \tau\nu_\tau) > 30\%$ . Note that the two-operator scenario with  $Re(C_{S_1})$  and  $Re(C_{S_2})$  is only marginally allowed as most of the parameter space, allowed by the  $B \rightarrow D^*\tau\nu_\tau$  and  $B \rightarrow D\tau\nu_\tau$  data, are disfavored by the limit on  $\mathcal{B}(B_c \rightarrow \tau\nu_\tau)$ . The two-dimensional posterior distributions for cases 7, 11, and 12 are found to be multi-modal i.e., there are multiple allowed regions in the NP parameter space.

A note here: as can be clearly seen from the plots, the multiple modes of cases 11 and 12 are fairly disconnected and separated from each other. As a result, the Markov-Chain-Monte-Carlo (MCMC) process, which samples the parametric distributions, has a fair chance to get stuck at one of these modes. Though this can be avoided using some parallel-tempering method [43] or an affine-invariant ensemble sampler [44], we instead have chosen to show the 1 and  $4\sigma$  confidence intervals obtained from the frequentist analysis. The solid and dashed contours in figures 5f and

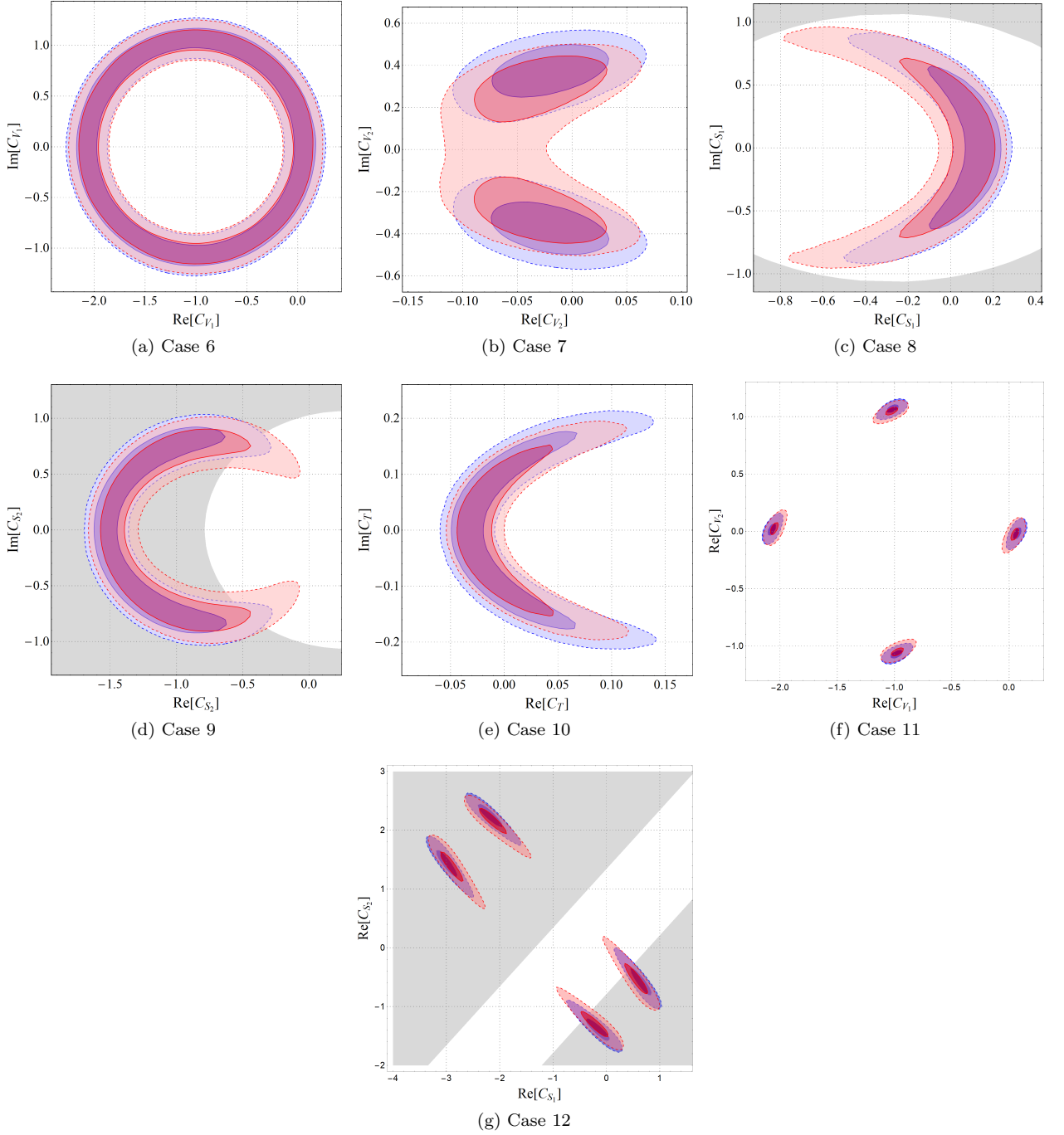


FIG. 5: Two-dimensional posterior distributions for the two parameter NP scenarios in tables VII and VIII. Blue shaded regions correspond to the NP fits to all the experimental inputs in table VI while the red shaded regions correspond to the fits after dropping BaBar data. Solid and dashed contours enclose respectively 68% and 95% highest probability regions for figures 5a - 5e, and 1 and  $4\sigma$  CLs for figures 5f and 5g. The gray shaded region denote the NP parameter space disallowed by  $\mathcal{B}(B_c \rightarrow \tau\nu_\tau) > 30\%$ .

5g enclose the 1 and  $4\sigma$  confidence intervals respectively. On the other hand, Figure 6 only shows the 68% and 95% Bayesian credible intervals for the mode that corresponds to the smallest absolute values for the WCs for the cases 11 and 12. As can be seen from these plots, the regions obtained from frequentist and Bayesian analyses are consistent. The nature of correlations are found to be mostly consistent with those in ref. [23], which does a similar NP analysis with CLN parametrization using the old Belle data [7]. These results could be utilized to extract the couplings and masses of different NP models.

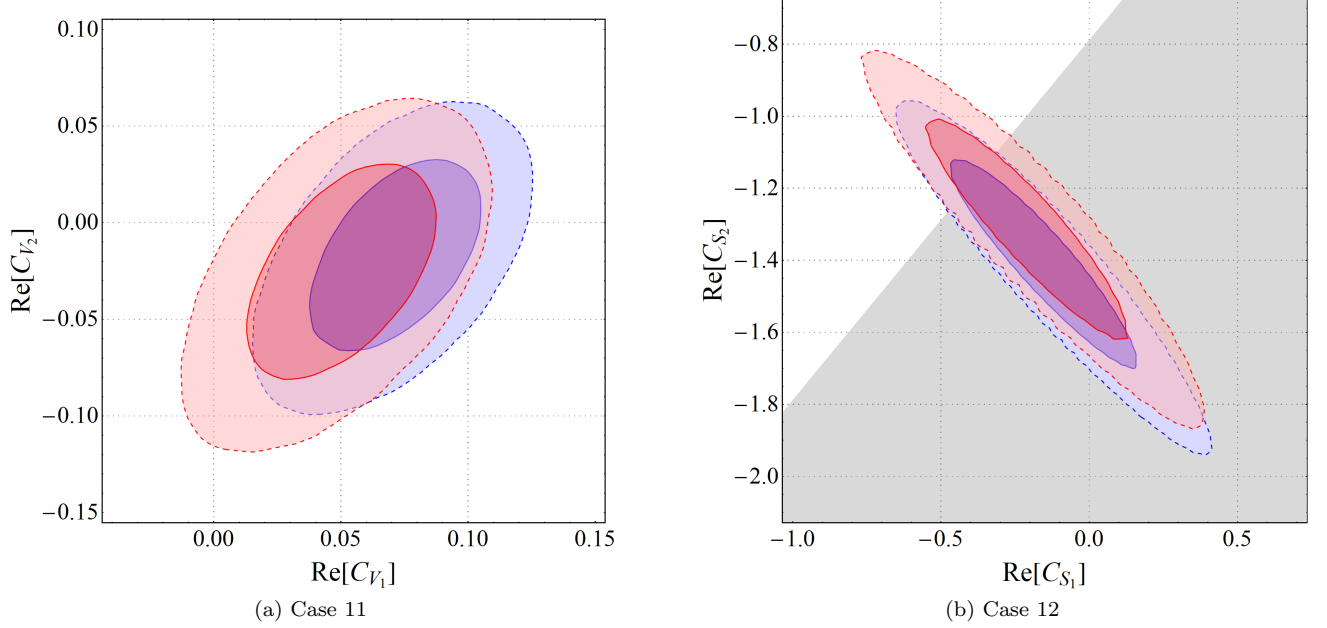


FIG. 6: Allowed NP parameter space for the multi-modal New Physics scenarios, with the smallest absolute values for the WCs. The blue shaded regions correspond to the NP fits to all the experimental inputs in table VI while the red shaded regions correspond to the fits after dropping BaBar data. Solid and dashed contours enclose 68% and 95% highest probability regions respectively. The gray shaded region denote the NP parameter space disallowed by  $\mathcal{B}(B_c \rightarrow \tau\nu_\tau) > 30\%$ .

Case	New WCs	$P_\tau(D)$	$A_{FB}(D)$	$P_\tau(D^*)$	$F_L(D^*)$	$A_{FB}(D^*)$
1	$\mathcal{R}e[C_{V_1}]$	0.326 (3)	0.3596 ( $\frac{3}{4}$ )	-0.488 ( $\frac{23}{25}$ )	0.471 ( $\frac{9}{11}$ )	-0.034 (22)
2	$\mathcal{R}e[C_{V_2}]$	0.326(3)	0.3596 (4)	-0.164 ( $\frac{31}{30}$ )	0.482(10)	0.0001 ( $\frac{203}{200}$ )
3	$\mathcal{R}e[C_{S_1}]$	0.464 ( $\frac{35}{33}$ )	0.3597 ( $\frac{4}{3}$ )	-0.432 ( $\frac{29}{31}$ )	0.492 ( $\frac{11}{12}$ )	-0.004 ( $\frac{23}{21}$ )
5	$\mathcal{R}e[C_T]$	0.348(6)	0.344 (4)	-0.455 (20)	0.453 ( $\frac{9}{11}$ )	0.008 ( $\frac{18}{17}$ )
6	$\mathcal{R}e[C_{V_1}], \mathcal{I}m[C_{V_1}]$	0.325 ( $\frac{2}{3}$ )	0.3597 ( $\frac{4}{3}$ )	-0.488 ( $\frac{24}{25}$ )	0.474 ( $\frac{13}{8}$ )	-0.032 ( $\frac{24}{20}$ )
7	$\mathcal{R}e[C_{V_2}], \mathcal{I}m[C_{V_2}]$	0.326 ( $\frac{3}{2}$ )	0.3596 ( $\frac{3}{4}$ )	-0.184 ( $\frac{32}{29}$ )	0.473 ( $\frac{11}{10}$ )	0.012 ( $\frac{18}{19}$ )
8	$\mathcal{R}e[C_{S_1}], \mathcal{I}m[C_{S_1}]$	0.471 ( $\frac{36}{32}$ )	0.3597 ( $\frac{4}{3}$ )	-0.439 ( $\frac{32}{27}$ )	0.487 ( $\frac{12}{14}$ )	-0.014 ( $\frac{22}{25}$ )
10	$\mathcal{R}e[C_T], \mathcal{I}m[C_T]$	0.343 ( $\frac{32}{10}$ )	0.348 ( $\frac{6}{17}$ )	-0.437 ( $\frac{31}{69}$ )	0.445 ( $\frac{34}{16}$ )	0.014 ( $\frac{20}{17}$ )
11	$\mathcal{R}e[C_{V_1}], \mathcal{R}e[C_{V_2}]$	0.326(3)	0.3597 ( $\frac{4}{3}$ )	-0.490 ( $\frac{24}{25}$ )	0.472 ( $\frac{10}{11}$ )	0.303 ( $\frac{21}{20}$ )

TABLE IX: Predictions for various angular observables for the allowed New Physics scenarios in table VII using the fit to all the experimental inputs.

In table IX, we have shown the predicted values of the angular observables associated with the all data (including BaBar) from  $B \rightarrow D^*\tau\nu_\tau$  and  $B \rightarrow D\tau\nu_\tau$  decays (table VI) for all the allowed NP scenarios (table VII). If we instead use the fit with both experimental and lattice inputs from  $B \rightarrow D\ell\nu_\ell$  decay (for details, see ref. [15]), we get the Standard Model estimates :  $P_\tau(D) = 0.326(3)$  and  $A_{FB}(D) = 0.3596(3)$ . Note that the predicted values of  $P_\tau(D)$  are different (slightly higher) in the scenarios with left-handed scalar current (with WC ‘ $C_{S_1}$ ’) than the other scenarios. Similar observation can be made for  $P_\tau(D^*)$  in the scenario with right-handed vector current with the WC ‘ $C_{V_2}$ ’. In this scenario, the magnitude of the predicted value is much lower than those of the predictions in other scenarios. Therefore, the precise measurements of these observables will be helpful to pinpoint these specific NP scenarios. Also, while the predicted values of  $F_L(D^*)$  in all the NP scenarios are consistent with the experimental result at  $2\sigma$ , their central values are much lower than the corresponding measured value.

IV.  $R(D^*)$  USING THE PRELIMINARY LATTICE INPUTS AT NON-ZERO RECOILS

Parameters	Fit to JLQCD data[32]	Fit to MILC data[31]
	+ LCSR data [20] + $h_{A_1}(1)$ from MILC [4]	+ LCSR data [20] + $h_{A_1}(1)$ from MILC [4]
$a_0^f$	0.0120(1)	0.0125(1)
$a_1^f$	-0.0084 ( $\frac{144}{143}$ )	0.0087(186)
$a_2^f$	0.1730(4082)	-0.2684(3802)
$a_1^{\mathcal{F}1}$	-0.0015 ( $\frac{30}{31}$ )	-0.0040 ( $\frac{32}{34}$ )
$a_2^{\mathcal{F}1}$	0.0885 ( $\frac{638}{566}$ )	0.0769 ( $\frac{708}{750}$ )
$a_0^g$	0.0299(4)	0.0329(6)
$a_1^g$	-0.0634 ( $\frac{481}{476}$ )	-0.1407 ( $\frac{826}{784}$ )
$a_2^g$	-0.0285(5667)	0.0173(5658)
$a_0^{\mathcal{F}2}$	0.0478(19)	0.0505(12)
$a_2^{\mathcal{F}2}$	0.0192(5674)	-0.0072(5646)

TABLE X: The values of the BGL coefficients (N=2) which are extracted using the preliminary lattice results on form-factors beyond zero-recoil from MILC collaboration [31] and JLQCD [32]. In both the analysis, LCSR inputs[20] for  $q^2 = 0$  are used and  $h_{A_1}(1) = 0.906(13)$  is taken from unquenched Fermilab/MILC lattice data [4].

Inputs used in the fit	JLQCD data[32] + LCSR data [20] + $h_{A_1}(1)$ from MILC [4]				MILC data[31] + LCSR data [20] + $h_{A_1}(1)$ from MILC [4]			
	Observable	$R(D^*)$	$P_\tau^{(D^*)}$	$F_L^{D^*}$	$A_{FB}^{(D^*)}$	$R(D^*)$	$P_\tau^{(D^*)}$	$F_L^{D^*}$
Value	0.244	-0.500	0.458	-0.051	0.251	-0.507	0.443	-0.062
Error	0.012	( $\frac{+0.014}{-0.012}$ )	0.011	( $\frac{+0.012}{-0.011}$ )	0.012	( $\frac{+0.010}{-0.013}$ )	0.010	( $\frac{+0.012}{-0.011}$ )
Correlation Matrix	1	-0.885	-0.792	-0.780	1	-0.911	-0.854	-0.739
		1	0.956	0.917		1	0.959	0.834
			1	0.954			1	0.911
				1				1

TABLE XI: Predictions and the correlations for the observables in  $B \rightarrow D^* \tau \nu_\tau$  decays corresponding to the fits of Table X.

As mentioned in the introduction, lattice collaborations, like JLQCD and Fermilab MILC, are analyzing the form-factors associated with the above mentioned decays at non-zero recoil. They have shown their preliminary results on this in a couple of conference proceedings [31, 32]. In this section, we do a toy analysis to study the impact of these preliminary lattice results on the  $B \rightarrow D^* \ell \nu_\ell$  form-factors. In this part of the analysis, we are neither using any experimental inputs, nor inputs from HQET to constrain the form-factors in  $B \rightarrow D^* \ell \nu_\ell$  and  $B \rightarrow D^* \tau \nu_\tau$ . Rather, the obtained predictions are totally dependent on the inputs from lattice and LCSR. The extracted values of the form-factors from these fits and the various predictions obtained using them can then be compared to those with the experimental inputs. Since the results are preliminary, we have not used them to extract  $V_{cb}$ , but have given a preliminary prediction of  $R(D^*)$ .

In the rest of this section, we discuss the details of our method of analysis. For lattice inputs from JLQCD [32], we extract nine lattice data-points for each of the four HQET form factors ( $h_V(w)$ ,  $h_{A_1}(w)$ ,  $h_{A_2}(w)$ , and  $h_{A_3}(w)$ ) corresponding to nine  $w$  values ( $w = 1, 1.01, 1.02, 1.03, 1.04, 1.05, 1.08, 1.09$ , and  $1.10$ ), i.e., a total of 36 data-points. For the inputs from MILC [31], we extract five lattice data-points for each of the four HQET form factors corresponding

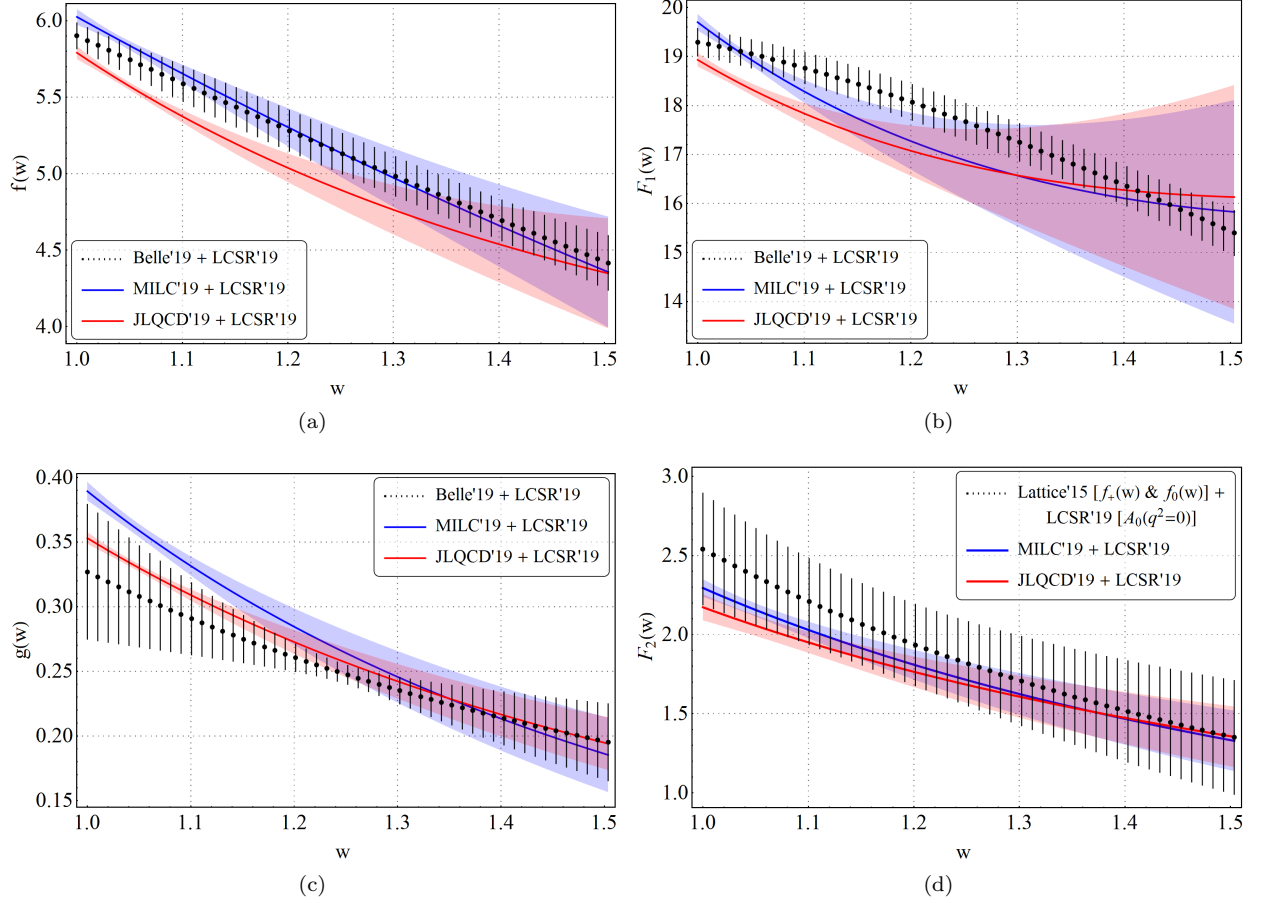


FIG. 7: In figures 7a - 7c, the shape of  $B \rightarrow D^*$  BGL form factors for  $N = 2$  obtained from the fit to new Belle data [17] (black bars) is compared to the preliminary lattice inputs from MILC [31] (blue band) and the lattice inputs from JLQCD [32] (red band) together with LCSR inputs [20]. In figure 7d, the blue and red bands hold the same meaning in context to  $F_2$  while the black bars represent  $F_2$  obtained using the method discussed in section II B.

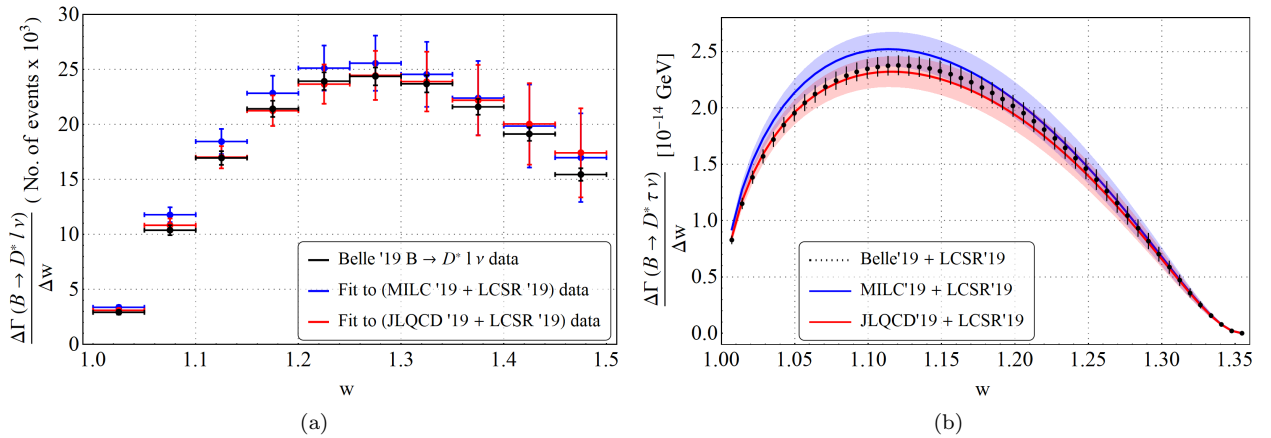


FIG. 8: (a) Comparison of the  $B \rightarrow D^* l \nu_\ell$  decay distributions in  $w$ -bins between theory and experiment. The black error-bars represent the latest experimental data from Belle [17]. In the case of theory, the form-factors are extracted using the preliminary inputs from table X. (b) Differential decay-distributions for  $B \rightarrow D^* \tau \nu_\tau$  decays. The black bars correspond to our fit results with Belle 2019 data and LCSR (and using the HQET relations between the form-factors as explained in section II B). Other two color codes are same as in figure (a).

to five  $w$  values ( $w = 1, 1.02, 1.04, 1.06$ , and  $1.08$ ), i.e., a total of 20 data-points. The HQET form-factors can be easily expressed in terms of the BGL form-factors ( $g(w)$ ,  $f(w)$ ,  $F_1(w)$ , and  $F_2(w)$ ). Thus, we can easily extract all the required BGL coefficients and form-factors using these preliminary lattice results. Fit results for all four  $B \rightarrow D^* \ell \nu_\ell$  BGL form factors for  $N = 2$  using the JLQCD and MILC data-points are given in the second and third columns of table X respectively. In both of these fits, LCSR inputs [20] for  $q^2 = 0$  are used in addition as well. For  $h_{A_1}(1)$ , the result from unquenched Fermilab/MILC lattice data [4] ( $h_{A_1}(1) = 0.906(13)$ ) is used instead of the preliminary MILC [31] and JLQCD [32] results. Since we can directly extract  $F_2(z)$  using lattice in this case, there is no need to use the HQET relations between the form-factors. Using these results, the prediction of  $R(D^*)$  and other important observables is straight-forward and they are given in Table XI along-with their correlations. Comparing these results with the ones given in table V, we note that all the respective predictions are consistent with each other within the error-bars. Though the central value of  $R(D^*)$  obtained from JLQCD results is slightly lower than the that found using the other inputs, at the moment it still has large uncertainty. We have to wait for the final conclusion till we get the final results with complete error budget.

Figure 7 compares the shape of the form-factors at different values of  $w$ . The plots are generated using the above mentioned preliminary lattice results at non-zero recoils, and these are compared with the one extracted in our earlier analysis using experimental results and LCSR. For all the form-factors except  $F_2$ , the JLQCD and MILC results differ from each other near the zero recoil, which is evident from their data as well. We have used LCSR inputs at  $q^2 = 0$ , and thus the shape of the form-factors across all the fits agree with each other at the maximum recoil. Considering the uncertainties at  $2\sigma$  CI in the form-factors extracted from experimental data, they agree with the respective JLQCD and MILC predictions then at lower values of recoil. In the case of  $F_2$ , apart from the preliminary results from JLQCD and MILC, the form-factors are extracted using lattice results on  $f_+$  and  $f_0$  and LCSR without any inputs from experiments. As we can see from figure 7d, the  $w$ -distributions are agreeing with each other in all the three cases.

In figure 8, we have compared the decay-rate distributions in  $w$ -bins for the decays  $B \rightarrow D^* \ell \nu_\ell$  (figure 8a) and  $B \rightarrow D^* \tau \nu_\tau$  (figure 8b) for different scenarios. We note that the results obtained from the preliminary lattice results are in good agreement with each other and also with the corresponding experimental results from Belle [17]. Any further conclusion needs to wait for more complete results from the lattice. In the case of  $B \rightarrow D^* \tau \nu_\tau$  decays, we find good agreement between the distributions obtained from JLQCD and MILC, and they also agree with one of the earlier fits in table V (last column). So far, all the predictions in the SM, obtained with or without the explicit use of experimental results in  $B \rightarrow D^* \ell \nu_\ell$ , are consistent with each other.

## V. SUMMARY

In this article, we have reanalyzed the  $B \rightarrow D^* \ell \nu_\ell$ , and  $B \rightarrow D^* \tau \nu_\tau$  decays on the basis of new Belle data and have updated the extracted values of  $|V_{cb}|$  and  $R(D^*)$  in the SM. We have done the analysis with and without the inputs from LCSR at  $q^2 = 0$ . Our new results *without* LCSR are:

$$\begin{aligned} |V_{cb}| &= 39.37_{-1.21}^{+1.07} \times 10^{-3} \\ \text{and } R(D^*) &= 0.251_{-0.005}^{+0.004}, \end{aligned} \quad (9)$$

and *after incorporating* LCSR, we get:

$$\begin{aligned} |V_{cb}| &= 39.56_{-1.06}^{+1.04} \times 10^{-3} \\ \text{and } R(D^*) &= 0.252_{-0.007}^{+0.006}. \end{aligned} \quad (10)$$

We note that compared to our 2017 analysis [15], the respective uncertainties in both  $|V_{cb}|$  and  $R(D^*)$  have reduced considerably, and they are consistent with each other within the error-bars. We have also predicted several angular observables associated with the  $B \rightarrow D^* \tau \nu_\tau$  decays. The SM predictions for  $F_L(D^*)$  is consistent with the respective measurement at  $2\sigma$ . Also, the value is lower than the corresponding measured value.

The above predictions of  $R(D^*)$  are not entirely consistent with the measured values. This excess can be explained in a model-independent way by assuming the presence of some new vector, scalar or tensor-type operators. We have worked out the constraints on the new Wilson coefficients associated with such new operators. The analysis and the resultant parameter spaces of the allowed scenarios show that the data still allow large new physics contributions in those decay modes. We note that the NP scenarios with right-handed scalar quark current are disfavored by the data and the most favored scenario is the one with left-handed vector quark current operator (SM type).

Very recently, lattice collaborations like Fermilab MILC and JLQCD have presented their preliminary results on the HQET form-factors at non-zero recoil. To do a consistency check, we have predicted  $R(D^*)$  using only those

results. The obtained values are consistent with the one mentioned above. Also, the extracted form-factors and the decay rate distributions in  $B \rightarrow D^* \ell \nu_\ell$  and  $B \rightarrow D^* \tau \nu_\tau$  are compared with the one obtained from the analysis with experimental data on  $B \rightarrow D^* \ell \nu_\ell$  as inputs. In the case of  $B \rightarrow D^* \ell \nu_\ell$  decays, we do not find any discrepancy between the experimental results of the w-rate distributions and those obtained using preliminary lattice results at non-zero recoil. Similarly, in the case of  $B \rightarrow D^* \tau \nu_\tau$  decay, results obtained from JLQCD and Fermilab-MILC are in good agreement to that from fitting the data with lattice and LCSR together. More concrete results with appropriate error budgets are needed from the lattice groups for any further conclusion.

## VI. ACKNOWLEDGMENT

### Acknowledgments

We would like to thank Alejandro Vaquero Avils-Casco for useful discussions. This project and S.N. is supported by the Science and Engineering Research Board, Govt. of India, under the grant CRG/2018/001260.

- 
- [1] A. Alberti, P. Gambino, K. J. Healey, and S. Nandi, Phys. Rev. Lett. **114**, 061802 (2015), 1411.6560.  
[2] P. Gambino, K. J. Healey, and S. Turczyk, Phys. Lett. **B763**, 60 (2016), 1606.06174.  
[3] Y. Amhis et al. (HFLAV), Eur. Phys. J. **C77**, 895 (2017), 1612.07233.  
[4] J. A. Bailey et al. (Fermilab Lattice, MILC), Phys. Rev. **D89**, 114504 (2014), 1403.0635.  
[5] J. A. Bailey et al. (MILC), Phys. Rev. **D92**, 034506 (2015), 1503.07237.  
[6] H. Na, C. M. Bouchard, G. P. Lepage, C. Monahan, and J. Shigemitsu (HPQCD), Phys. Rev. **D92**, 054510 (2015), [Erratum: Phys. Rev.D93,no.11,119906(2016)], 1505.03925.  
[7] A. Abdesselam et al. (Belle) (2017), 1702.01521.  
[8] C. G. Boyd, B. Grinstein, and R. F. Lebed, Phys. Rev. **D56**, 6895 (1997), hep-ph/9705252.  
[9] I. Caprini, L. Lellouch, and M. Neubert, Nucl. Phys. **B530**, 153 (1998), hep-ph/9712417.  
[10] D. Bigi and P. Gambino, Phys. Rev. **D94**, 094008 (2016), 1606.08030.  
[11] D. Bigi, P. Gambino, and S. Schacht, Phys. Lett. **B769**, 441 (2017), 1703.06124.  
[12] B. Grinstein and A. Kobach, Phys. Lett. **B771**, 359 (2017), 1703.08170.  
[13] F. U. Bernlochner, Z. Ligeti, M. Papucci, and D. J. Robinson, Phys. Rev. **D95**, 115008 (2017), [erratum: Phys. Rev.D97,no.5,059902(2018)], 1703.05330.  
[14] D. Bigi, P. Gambino, and S. Schacht, JHEP **11**, 061 (2017), 1707.09509.  
[15] S. Jaiswal, S. Nandi, and S. K. Patra, JHEP **12**, 060 (2017), 1707.09977.  
[16] Heavy Flavor Averaging Group, *Updates of Semileptonic Results for Spring 2019*, <https://hflav-eos.web.cern.ch/hflav-eos/semi/spring19/main.shtml> (2019), [Online; accessed 11-February-2020].  
[17] E. Waheed et al. (Belle), Phys. Rev. **D100**, 052007 (2019), 1809.03290.  
[18] P. Gambino, M. Jung, and S. Schacht, Phys. Lett. **B795**, 386 (2019), 1905.08209.  
[19] M. Bordone, M. Jung, and D. van Dyk, Eur. Phys. J. **C80**, 74 (2020), 1908.09398.  
[20] N. Gubernari, A. Kokulu, and D. van Dyk, JHEP **01**, 150 (2019), 1811.00983.  
[21] F. U. Bernlochner, Z. Ligeti, and D. J. Robinson, Phys. Rev. **D100**, 013005 (2019), 1902.09553.  
[22] S. Bhattacharya, S. Nandi, and S. K. Patra, Phys. Rev. **D95**, 075012 (2017), 1611.04605.  
[23] S. Bhattacharya, S. Nandi, and S. Kumar Patra, Eur. Phys. J. **C79**, 268 (2019), 1805.08222.  
[24] S. Bhattacharya, A. Biswas, S. Nandi, and S. K. Patra (2019), 1908.04835.  
[25] F. Feruglio, P. Paradisi, and O. Sumensari, JHEP **11**, 191 (2018), 1806.10155.  
[26] Z.-R. Huang, Y. Li, C.-D. Lu, M. A. Paracha, and C. Wang, Phys. Rev. **D98**, 095018 (2018), 1808.03565.  
[27] M. Blanke, A. Crivellin, S. de Boer, T. Kitahara, M. Moscati, U. Nierste, and I. Niandi, Phys. Rev. **D99**, 075006 (2019), 1811.09603.  
[28] C. Murgui, A. Peuelas, M. Jung, and A. Pich, JHEP **09**, 103 (2019), 1904.09311.  
[29] P. Asadi and D. Shih, Phys. Rev. **D100**, 115013 (2019), 1905.03311.  
[30] R.-X. Shi, L.-S. Geng, B. Grinstein, S. Jger, and J. Martin Camalich, JHEP **12**, 065 (2019), 1905.08498.  
[31] A. V. Avils-Casco, C. DeTar, A. X. El-Khadra, A. S. Kronfeld, J. Laiho, and R. S. Van de Water (Fermilab Lattice, MILC), in *37th International Symposium on Lattice Field Theory (Lattice 2019) Wuhan, Hubei, China, June 16-22, 2019* (2019), 1912.05886, URL <https://lss.fnal.gov/archive/2019/conf/fermilab-conf-19-633-t.pdf>.  
[32] T. Kaneko, Y. Aoki, G. Bailas, B. Colquhoun, H. Fukaya, S. Hashimoto, and J. Koponen (JLQCD), in *37th International Symposium on Lattice Field Theory (Lattice 2019) Wuhan, Hubei, China, June 16-22, 2019* (2019), 1912.11770.  
[33] S. Hirose et al. (Belle), Phys. Rev. Lett. **118**, 211801 (2017), 1612.00529.  
[34] A. Abdesselam et al. (Belle), in *10th International Workshop on the CKM Unitarity Triangle (CKM 2018) Heidelberg, Germany, September 17-21, 2018* (2019), 1903.03102.  
[35] Y. Sakaki, M. Tanaka, A. Tayduganov, and R. Watanabe, Phys. Rev. **D88**, 094012 (2013), 1309.0301.

- [36] J. P. Lees et al. (BaBar), Phys. Rev. **D88**, 072012 (2013), 1303.0571.
- [37] M. Huschle et al. (Belle), Phys. Rev. **D92**, 072014 (2015), 1507.03233.
- [38] R. Aaij et al. (LHCb), Phys. Rev. Lett. **115**, 111803 (2015), [Erratum: Phys. Rev. Lett.115,no.15,159901(2015)], 1506.08614.
- [39] R. Aaij et al. (LHCb), Phys. Rev. Lett. **120**, 171802 (2018), 1708.08856.
- [40] A. Abdesselam et al. (Belle) (2019), 1904.08794.
- [41] G. Caria et al. (Belle) (2019), 1910.05864.
- [42] R. Alonso, B. Grinstein, and J. Martin Camalich, Phys. Rev. Lett. **118**, 081802 (2017), 1611.06676.
- [43] R. H. Swendsen and J.-S. Wang, Phys. Rev. Lett. **57**, 2607 (1986), URL <https://link.aps.org/doi/10.1103/PhysRevLett.57.2607>.
- [44] J. Goodman and J. Weare, Commun. Appl. Math. Comput. Sci. **5**, 65 (2010), URL <https://doi.org/10.2140/camcos.2010.5.65>.